Original article

Journal of High School Science

Force model and experimental analysis of a simple straw pump

Cheng-You Ho

Submitted: June 2, 2024, Revised: version 1, June 30, 2024
Accepted: July 1, 2024

Abstract
A low-cost centrifugal pump made by folding a straw into a triangle, immersing it into water and spinning it serves both as a DIY demonstration and as a pragmatic water sprinkler. A point-mass model is first examined to describe the dynamics of water droplets, with corrections due to Bernoulli's effect, surface tension and viscosity subsequently considered, where surface tension is found negligible. Effects of straw diameter, immersion depth, rotation angular velocity and tilt angle are discussed experimentally, which fit the predictions of the corrected point-mass model. The dependence of aerodynamic drag on droplet radii is discussed. For practical applications, the effect of p_{init} (pressure at the inlet) is evaluated, and it is also predicted that there exist conditions for maximum droplet range and exit velocity, providing insight into optimizing the setup for lawn or fire sprinklers.

Keywords
Physics, Mechanics, Fluid dynamics, Theoretical modeling, Mechanical pump, Centrifugal pump, Straw pump, Point mass model, Bernoulli's effect, Surface tension

Cheng-You Ho, National Chiayi Senior High School. No. 738, Section 2, Daya Rd, East District, Chiayi City, 600 Taiwan R.O.C. chengyou1368@gmail.com

Introduction

A DIY water sprinkler pump is of significant value due to its low cost and simplicity to assemble. Pumps can be categorized into displacement pumps and dynamic pumps. The latter category includes centrifugal pumps, which utilize centrifugal forces to achieve pumping. The working fluid, assumed to be water for the current system, enters the pump through the center, or the eye, of the impeller, the motor-driven part of the pump. With the impeller spinning, the water, when ejected along the tangential direction of the pump, acquires a high speed, therefore spraying water to farther locations (1). Homemade centrifugal pumps have been of great interest for nearly a century (2). However, most pumps are bulky and not practical for everyday use.

The straw pump is a simple STEM toy that functions as a centrifugal pump (3-4). The straw is folded (Figure 1 (a)) into a triangle with the openings glued together, as shown in Figure 1 (b). The other two vertices of the triangle are then joined to create openings for the working fluid to exit, as shown in Figure 1 (c). When one of the vertices of the triangle is immersed into water in an upright position and spun with respect to the symmetrical axis that is perpendicular to the water surface, water pumps out from the two top vertices. The simple water pump can be used to spray water radially. Though many sources (3-4) have indicated that the cause of this phenomenon, with respect to a non-inertial coordinate system, is the centrifugal force, a comprehensive quantitative analysis is currently absent in the literatue.

The apparatus is very similar to a fire sprinkler, with the water inlet is analogous to the base vertex of the triangular straw, the nozzle similar to the two sides, and the other two vertices of the straw functioning as the spray head. Hence, the system investigated here could motivate efficient designs for fire sprinklers.

This study investigates the motion of water by constructing a point-mass model and incorporating corrections due to fluid mechanics. An experiment is conducted to quantitatively verify the theory, which provides insight into the optimal design of the straw water pump.

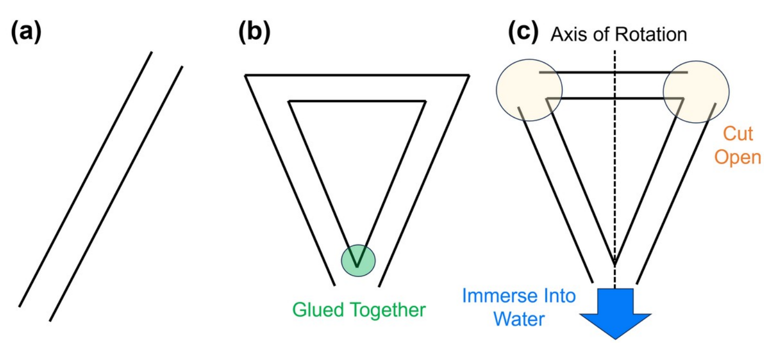

Figure 1. Schematic diagram of constructing the triangle straw. (a) A plastic straw. (b) The straw folded into a triangle with tips glued together. (c) The triangle cut at two vertices and immersed into water.

Materials and Methods

The apparatus is shown in Figure 2. The triangular straw, immersed into a plastic bucket of height 15.0 cm filled with tap water, was attached to the bottom of a rotating motor. A hose constantly supplied water to the bucket. The temperature of water was (22.0 ± 0.5) ºC, sourced from a direct faucet. During the experiment, the bucket was always kept filled to the brim with water with the constant water supply, so that the water level remained constant when pumping. There was no hindrance to the water spray from the walls of the bucket. A power supply provided 0 to 10 volts to the motor. The bucket was placed at the center of a large protractor. 50 cm rulers were placed radially outwards on the ground. A camera recording at 240 frames per second was located at the corner.

The experiment was performed by adjusting the output voltage of the power supply until water sprinkled out of the straw pump. The radial distance of the water droplets were measured using the rulers. Due to friction and the different straw dimensions used during the study, a simple relationship between voltage and the angular velocity of the motor could not be established. Therefore, the camera recorded the spinning motion of the straw, and the angular velocity was computed using the VLC Media Player by manually counting the average number of frames required for each rotation.

Seven different kinds of triangular straws were used. As shown in Figure 3, the straws have different diameters and side lengths. Except for the the triangular straw labeled E, which is an obtuse, isoseles triangle with the base angles ~ 41 degrees, all other triangles are equilateral. Figure 2 (b) shows various parameters of the straw pump system, including the angular velocity Ω around its axis of symmetry, straw diameter 2a, side length l, depth of immersion h_0 into the water surface, and the exit velocity of water droplets, v_0.

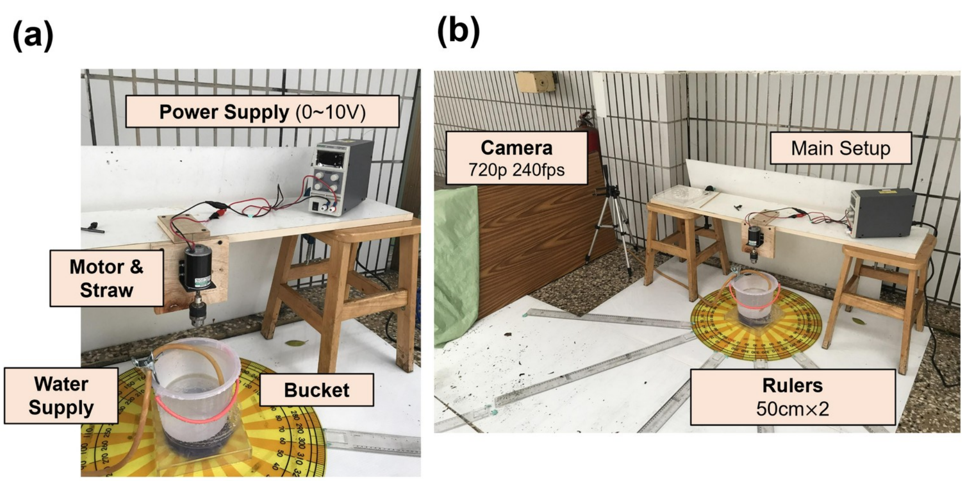

Figure 2. Experiment apparatus. (a) Close-up view of the straw pump system. (b) Relative positions of the camera and the main setup.

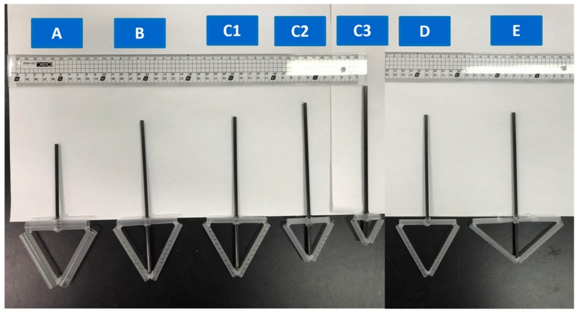

Label	$2a$ (mm)	l (cm)	l_{top} (cm)
A	12	7	7
B	8	7	7
C1	6	7	7
C2	6	5	5
C3	6	3	3
D	4	7	7
E	6	7	10.5

Figure 3. The 7 triangular straws of different dimensions used. where 2a is the diameter, l is the side length of the triangle, and l_{top} refers to the length of the base of the straw.

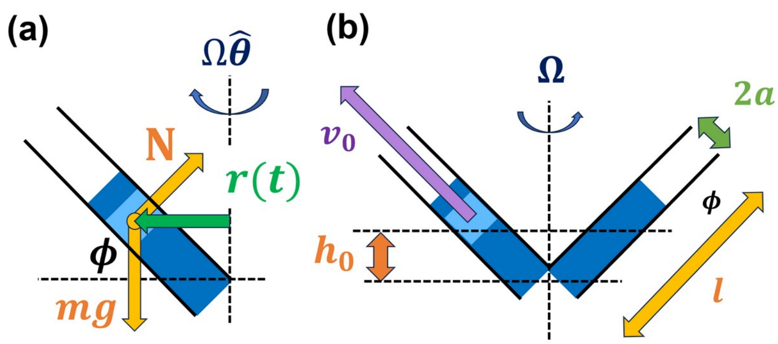

Figure 4. (a) Free body diagram of an infinitesimal water segment. (b) Parameters of the straw pump system.

Results and Discussion

Point-Mass Model

A simplified discussion of the motion of water inside the straw can be established by considering an infinitesimal water segment as a point mass. The discussion below is with respect to an inertial lab frame. The free body diagram is shown in Figure 4 (a), where the two forces acting on the cyan infinitesimal segment are those of gravity, mg, and the normal force, N provided by the walls of the straw. The cylindrical coordinate system is used, with the origin centered at the bottom vertex of the straw and the axis of rotation being the vertical z axis. The position of the water segment can be described using three variables: r(t), θ(t) and z(t). Due to the kinematic constraints of the straw,

$$\theta(t)=\Omega t,\ z(t)=r(t)\tan\varphi \tag{1}$$

must be satisfied at all times. Therefore, the full motion of the water segment can be solved by determining r(t). The equation of motion in the radial direction can be written as

$$m(\ddot{r} - r(\Omega \cos\phi)^2) = -N\sin\phi = -mg\sin\phi\cos\phi \quad (2)$$

Substituting the general solution (3) into equation (2), the equation of motion in the radial direction is obtained as equation (4). In equation (4), the term r_{0c} is given by equation (5).

$$r(t) = A'\sinh\Omega' t + B'\cosh\Omega' t + \frac{g\sin 2\phi}{2(\Omega\cos\phi)^2} \quad (3)$$

$$r(t) = (r_0 - r_{0c})\cosh\Omega' t + r_{0c} \quad (4)$$

$$r_{0c} = \frac{g\sin 2\phi}{2\Omega'^2} \quad (5)$$

is the minimum initial radial displacement for rising motion to occur; if the initial radial distance is too small, gravity dominates and the point mass slides down the straw. To solve for τ, the time that the infinitesimal water segment exits the straw, $r(\tau)$ is set equal to $l\cos(\theta)$, which gives

$$\tau = \frac{1}{\Omega'}\cosh^{-1}\left(\frac{l\cos\phi - r_{0c}}{r_0 - r_{0c}}\right) \quad (6)$$

Taking the derivative of r(t) and evaluating it at time t yields, assisted with kinematic constraints, the velocity along the straw v_{th} at which the point mass exits the straw

$$v_{th} = v(\tau) = \Omega(r_0 - r_{0c})\sqrt{\left(\frac{l\cos\phi - r_{0c}}{r_0 - r_{0c}}\right)^2 - 1} \quad (7)$$

Corrections due to fluid dynamics

Fluids exert many physical properties, such as Bernoulli's effect, surface tension, viscosity, etc. that we failed to account thus far in the simplified point-mass model. To apply the analysis above on the straw pump system, a value for the effective gravity g_{eff}, combining the effects of multiple fluid effects, is calculated and substituted for the acceleration due to gravity g in the point-mass model.

Bernoulli's effect states that energy is conserved between two points on the same streamline, where a pressure difference arises between the bottom of the straw and the point where the water exits the straw. Such a correction is estimated under the assumption that the flow speed of water at the bottom vertex of the straw is negligible, compared to the exit velocity. This statement is plausible due to the continuity equation, since water is coming in from all directions at the bottom but exits out in a small cross section. Also, since energy loss due to viscosity is negligible (as discussed later), conservation of energy can be assumed along the streamline. Thus, Bernoulli's equation can be written as

$$p_{init} = p_{exit} + \rho g l \sin\varphi + \rho v_{th}^2/2 \quad (8)$$

where ρ=1000 kg/m^3 is the density of water, and p_{init}, p_{exit} are pressures at the bottom and top of a streamline exiting the straw, respectively. The pressure difference contributes to the effective gravity. The water column in the straw experiences an upwards force caused by surface tension. The perimeter of contact is approximated by an ellipse of semi-major axis a/cosθ and semi-minor axis a. The upwards force is then calculated as

$$F\gamma = \gamma * \text{Perimeter of ellipse} * \cos\theta \quad (9)$$

Where θ is the contact angle and γ=0.072 N/m is the surface tension of water. The perimeter of the ellipse can be evaluated with Ramanujan's first approximation formula (5) using Python's Scipy library (6). The contact angle of water in plastic straws (7) of diameter on the order of 1 mm is very close to 90º. A more detailed calculation later in this paper shows that the effect of surface tension is negligible compared to that of the Bernoulli's effect. In addition, viscosity effects are taken into account with the Darcy–Weisbach equation

$$\frac{\Delta p}{l} = f_D \cdot \frac{\rho}{2} \cdot \frac{v_{1/2}^2}{2a} \quad (10)$$

where the characteristic flow speed is taken to be half the maximum flow speed $v_{1/2}$,=0.5v_{th} and the Darcy friction factor (8) f_D~10^{-1} can be calculated with the Kármán–Prandtl resistance equation.

As an approximate estimate of the fluid corrections, consider φ=60º, l=70 mm, a=3 mm and a typical exit velocity along the straw v=5 m/s. Bernoulli's effect gives rise to a pressure difference $\Delta p_{Bern}=\rho g l \sin\varphi+\rho v^2/2$=13 kPa, while for surface tension, γ*Perimeter = 0.072 N/m * 0.272 m = 2*10^{-3} N. Even with the unreasonable assumption that in (9), in order to make Fγ as large as possible, the pressure difference Δp_γ~$F\gamma/a^2$~200Pa is still two order of magnitudes smaller than the pressure difference attributed to Bernoulli's effect. Furthermore, according to other sources previously, cosθ=0. Therefore, the effects of surface tension can be reasonably neglected. The pressure difference arisen from viscosity $\Delta p_{visc}=f_D l \rho v^2/16a$=3.6 kPa, is of the same order of magnitude, but in the opposite direction, of the Bernoulli's effect.

Neglecting surface tension and assuming that the cross sectional area of the flow inside the straw is A_{eff}, the pressure difference caused by Bernoulli's and viscosity effects $\Delta p=\Delta p_{Bern}-\Delta p$-

$_{visc}$ amounts to an effective force $F_{eff}=A_{eff}\Delta p$ and an effective acceleration $F_{eff}/A_{eff}l\rho$. Hence the effective gravity is given by

$$g_{eff} = g - l(gl\sin\phi + \frac{1}{2}v^2 - \frac{f_D l}{16a}v^2) \tag{11}$$

Such a correction at Δp=10 kPa leads to $l\Delta p/\rho \sim$ 0.7 m/s^2, which is not insignificant compared to g=9.81 m/s^2.

Data processing

The exit velocity is determined experimentally by measuring the horizontal range of water droplets, which experience a drag force while airborne (9)

$$F_D = -\rho_{air}C_D A v^2 = -kv^2 \tag{12}$$

where ρ_{air}=1.293 kg/m^3 is the density of air (10), the drag coefficient is approximately C_D=0.47 for spherical objects, $A=\pi r^2$ is the cross-sectional area where r is the droplet radius, and v is the velocity of the droplet of mass m. Newton's second law reads

$$\begin{cases} m\ddot{x} = -k\dot{x}^2 \\ m\ddot{y} = -k\dot{y}^2 - ng \end{cases} \tag{13}$$

where n is the effective mass considering buoyancy, $n=m\left(1-\frac{\rho_{air}}{\rho}\right)\approx 0.999\,m \approx m$. The system of differential equations is solved for x(t) and y(t), which yields (11)

$$\begin{cases} x(t) = \frac{m}{k}\ln\left(\frac{v_{0x}k}{m}t+1\right) \\ y(t) = h - \frac{m}{k}\ln\frac{\cos\left(\tan^{-1}\frac{\sqrt{\frac{k}{m}}v_{0y}}{\sqrt{\frac{ng}{m}}}\right)}{\cos\left(\tan^{-1}\left(\frac{\sqrt{\frac{k}{m}}v_{0y}}{\sqrt{\frac{ng}{m}}} - t\frac{\sqrt{kng}}{m}\right)\right)} \end{cases} \tag{14}$$

Consider the components of the 3-dimensional exit velocity, which consists of the component $v=v_\perp+v_\parallel$ along the straw and $u=l\Omega\cos\varphi$, caused by rotation of the straw itself. From Figure 5 (a), the airborne time of a water droplet is determined solely by $v_\perp$. However, the range is relevant to the vector addition of the parallel component of the velocity along the straw $v_\parallel$ and the tangential velocity u. Thus, in equation (14), the initial velocities are identified as

$$\begin{cases} v_{0x} = \sqrt{u^2 + v_{\parallel}^2} = \sqrt{u^2 + v^2 \cos^2 \phi} \\ v_{0y} = v_{\perp} = v \sin \phi \end{cases} \tag{15}$$

With u and φ known, equation (14), which yields the range, is plotted using Python, and v from experiments is determined iteratively, by finding the best value of v that, considering air drag, yields the range closest to the experimental value up to a precision of 0.01 m/s. The droplet radius takes the estimated value of 1mm. The uncertainty while measuring the range contributes to the uncertainty of v.

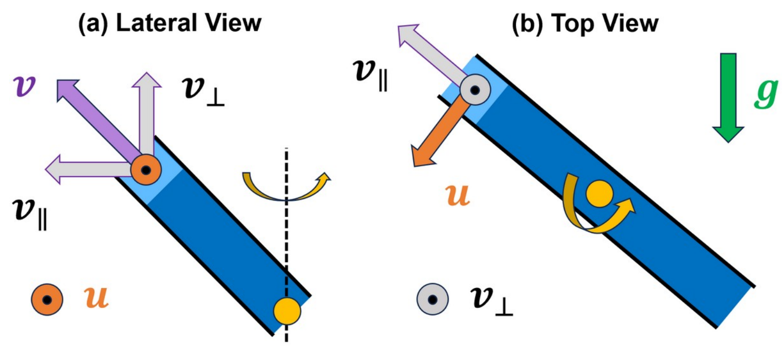

Figure 5. Components of the exit velocity, consisting of the component v along the straw and u, caused by rotation of the straw itself. The rotation axis is marked with a yellow dot, with the direction of rotation annotated by an yellow arrow. (a) Lateral view. (b) Top view.

Correlating theory and experiment
The theoretical predictions with and without fluid effect corrections are shown in Figure 6. It was found that the correction was insignificant. Although the effective gravity differs from the standard gravity significantly, the elapsed time of acceleration is too small for such a difference to produce an observable deviation, hence the exit velocity was dominated by centrifugal effects. It was also observed that at low angular velocities no fluid pumped out as the centrifugal force was too small, hence the "Ω-cutoff" as in Figure 6.

In Experiment 1, straw B was used and immersed into water at depths of 10 mm, 15 mm and 25 mm, with the v-Ω relationships plotted in Figure 7. The theory also predicted that the Ω-cutoff would be higher for larger immersion depths, though the differences in slope is seen to be relatively minor. The immersion depth of 25 mm was used in all subsequent experiments. For Experiment 2, straws A, B and C were used for different straw diameters of 6 mm, 8 mm and 12 mm, the v-Ω relationships plotted in Figure 8. The differences in theoretical predictions with different straw diameters was again, insignificant. Lastly, for experiment 3, the v-Ω relationship of the obtuse triangle E and the corresponding theory line is plotted in Figure 9 (a). It was found that theory lines vary significantly with the tilt angle as shown in Figure 9 (b).

It was concluded that the slopes of experimental data and theoretical predictions were similar. In almost all graphs, experiment data values were slightly larger by the theoretical prediction by 0.1~0.5 m/s. This may be due to the air pressure difference caused by fast-flowing air across the exit vertex of the straw. The calculation may require a complex understanding of the flow of air near such boundary. However, due to Bernoulli's effect, a low-pressure region near the exit vertex may be present, hence this is a possible explanation to the discrepancy between theory and experiment.

As shown in Figure 9, the exit velocity was largely dependent on φ. The dependence of exit velocity and droplet range on the tilt angle is plotted with sample parameters h_0=15 mm, l=7.0 cm, a=3 mm, Ω=70 rad/s in Figure 10. In the small-φ limit, centrifugal force dominated over gravity, but since the radial acceleration was larger, the time an infinitesimal water segment stayed within the straw is smaller, reducing both v_{exit} and range. Gravity dominated in the large-φ limit, therefore, similarly, lowered smaller v_{exit} and range. It is thus qualitatively plausible that there exists an extremum for the two quantaties as φ varies, which was indeed the case. Moreover, the effects of centrifugal force and gravity combined to create a maxima of the two quantities, though at different φ values since v_{exit} also took the component of velocity caused by the rotation of the triangular straw into account.

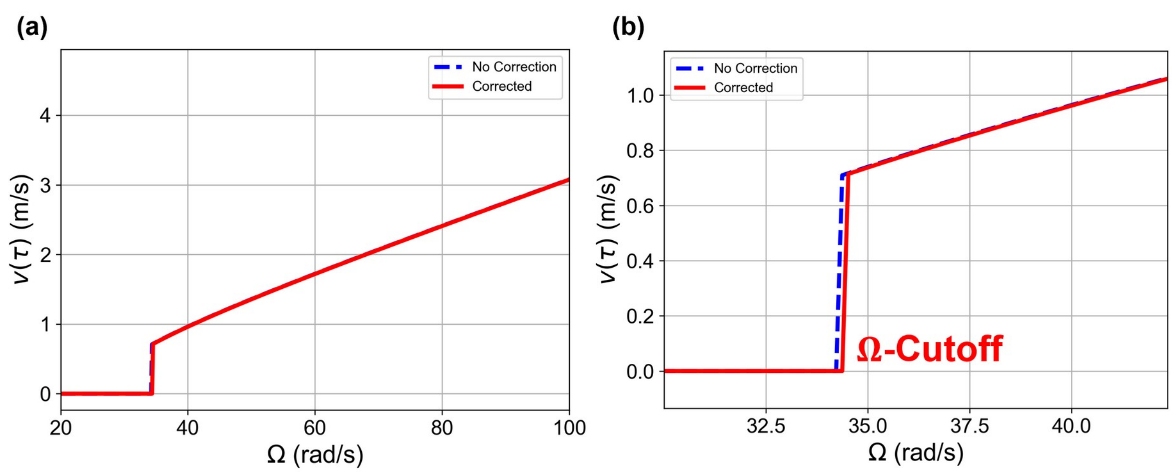

Figure 6. Theory v-Ω plot with (solid red) and without (dashed blue) the correction of fluid effects. The line is plotted with the parameters h_0=25 mm, l=7.0 cm, a=2 mm, φ=60 degrees. (a) The two curves are nearly indistinguishable. (b) Zooming in into the Ω-cutoff region reveals that the cutoff angular velocity is larger after the correction, though the effect of such correction at angular velocities above the cutoff is insignificant.

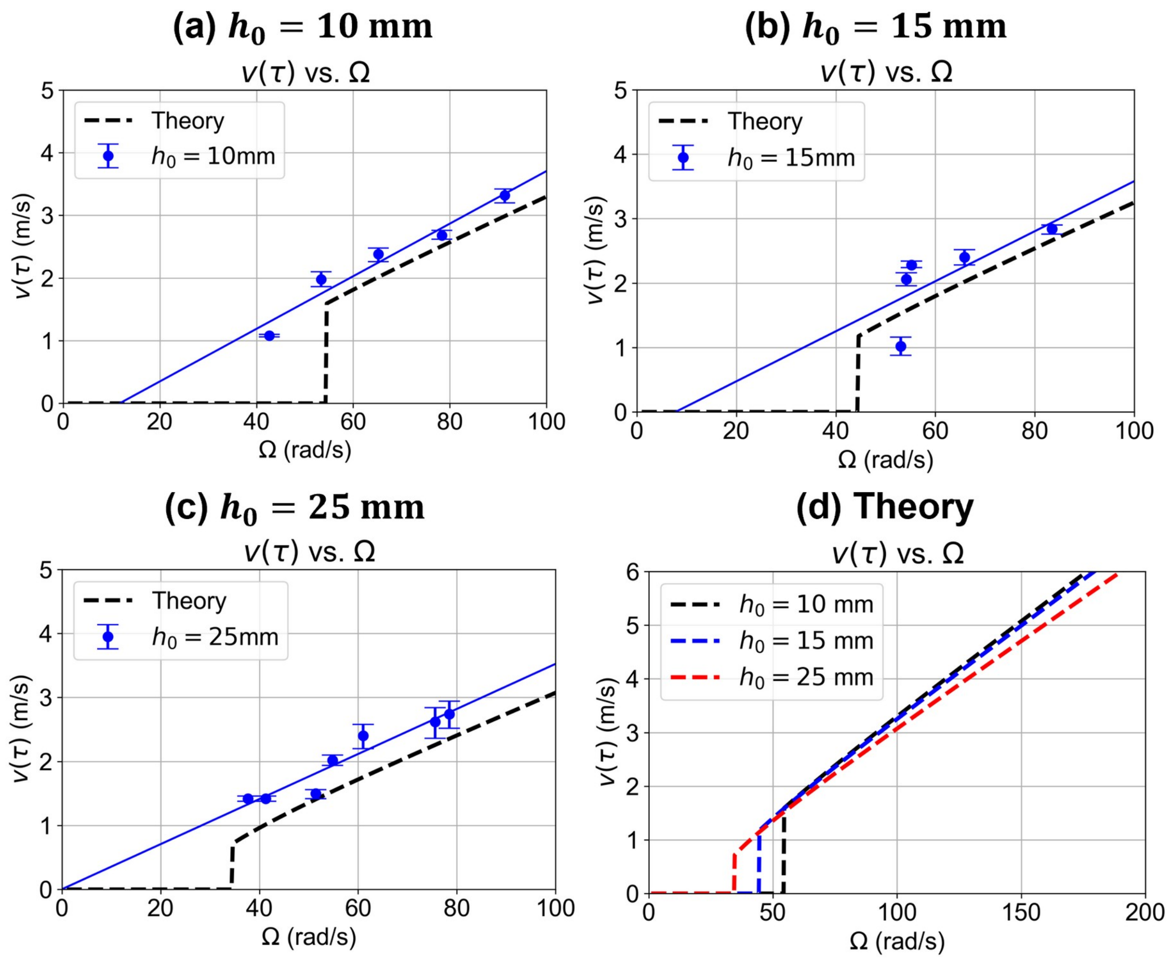

Figure 7. Experimental data and theoretical predictions of experiment 1. Experiment data of immersion depths (a) h_0=10 mm (b) h_0=15 mm and (c) h_0=25 mm are shown. Blue dots represent experiment data, the blue line is the linear fit of experimental data, and the dashed black line is the theoretical prediction. (d) Comparison of theory lines at different immersion depths.

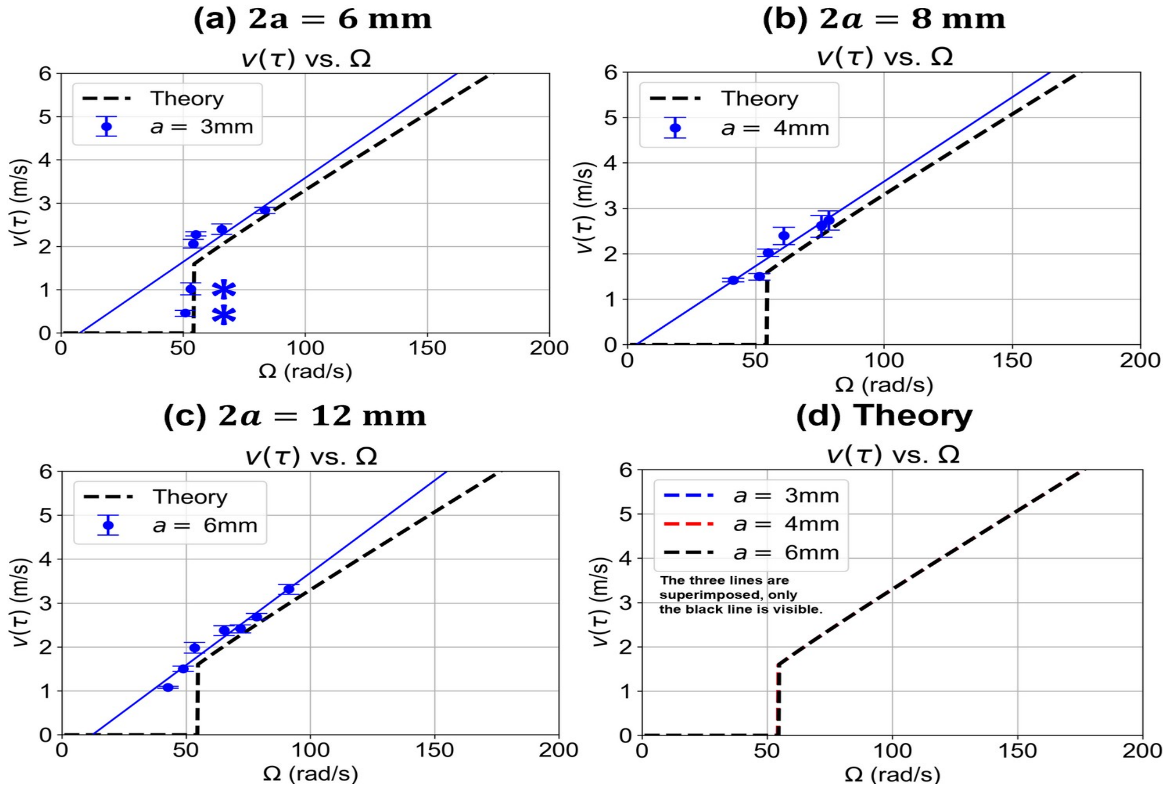

Figure 8. Experimental data and theoretical predictions of experiment 2. Experiment data of straw diameters (a) 2a=6 mm (b) 2a=8 mm and (c) 2a=12 mm are shown. Blue dots represent experiment data, the blue line is the linear fit of experimental data, and the dashed black line is the theoretical prediction. The two points marked with an asterisk are not used in the linear regression. (d) Comparison of theory lines at different straw diameters. The blue, red and black plots are superimposed, hence only the black line is visible.

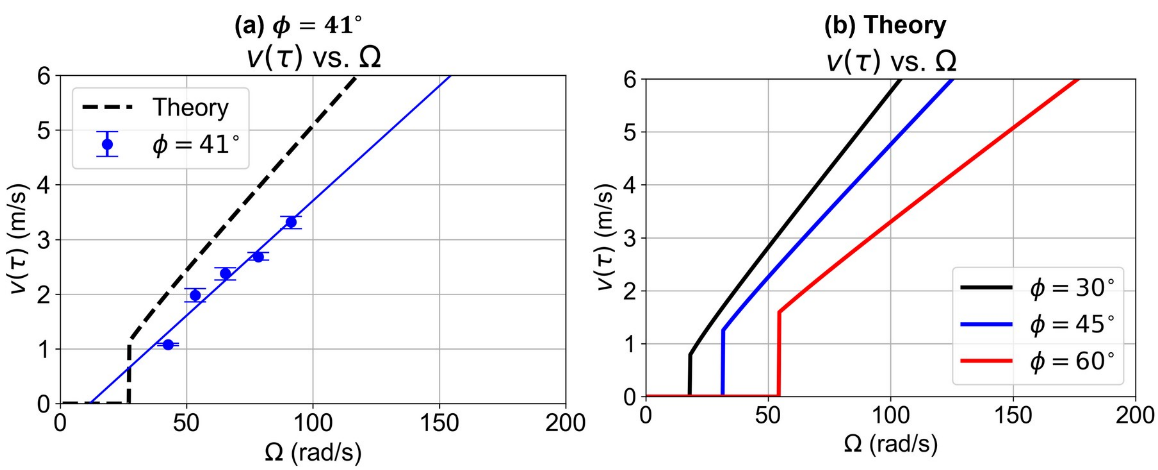

Figure 9. Experimental data and theoretical predictions of experiment 3. (a) Comparison of experiment and theory for straw E with tilt angle φ=41 degrees. Blue dots represent experiment data, the blue line is the linear fit of experimental data, and the dashed black line is the theoretical prediction. (d) Comparison of theory lines at different tilt angles.

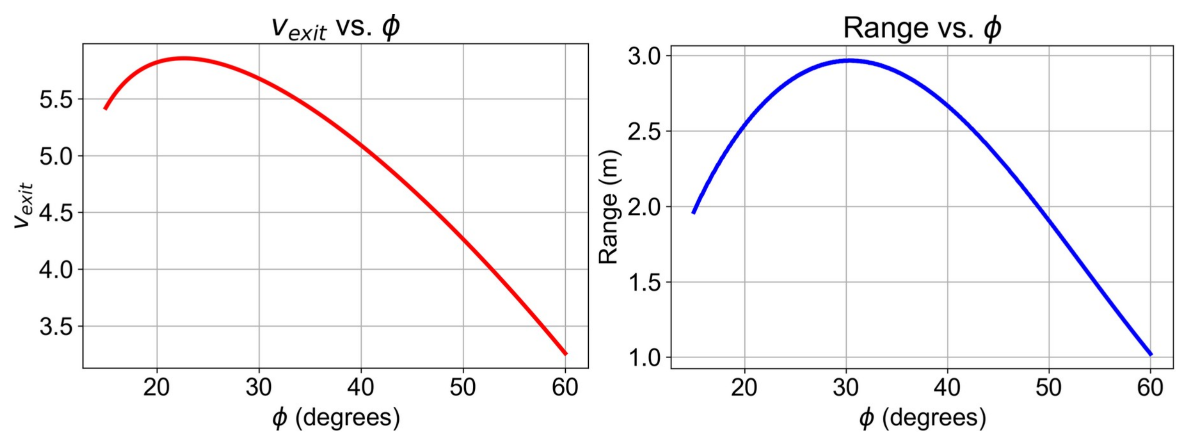

Figure 10. Theoretical dependence of exit velocity and range on tilt angle φ. The parameters used for plotting are h_0=15 mm, l=7.0 cm, a=3 mm, Ω=70 rad/s. Both quantaties depend largely on φ with a maximum on the respective curves.

The Ω-cutoff is relevant to immersion depth and straw diameter. Also, the ability to obtain the tilt angle that optimizes droplet range enables the theory to contribute to practical uses, such as water sprinkling, where the range usually needs to be maximized.

The y-intercept of the best fit line of experimental data for all experiments seemed to be close to the origin, while that of Figure 7 (c) passed through the origin. According to equation (7), which relates v_{th} to Ω, at the y-intercept where Ω=0, v_{th}=0. The relationship between v_{th} and Ω is not a simple relationship, since r_{0c} is dependent on Ω, according to equation (5), which can be observed by noting that plots of the theoretical relationship between v_{th} and Ω are slightly curved near the Ω-cutoff throughout this paper. Furthermore, below the Ω-cutoff, water cannot exit the straw, so it is physically impossible to obtain data at Ω=0. Hence, the y-intercept of the best fit line of experimental data does not contain a simple physical meaning. However, when Ω is large, r_{0c} approaches 0, according to equation (5), and the expression inside the radical of equation (7) approaches a constant, and v_{th} will be proportional to Ω. Therefore, the best fit line of experimental data at large enough Ω should pass through the origin. The fact that the best fit line of Figure 7 (c) passed through the origin, while all the other plots did not, should hence be treated as experimental error.

The droplet radius of 1mm was used to iteratively find the exit velocity experimentally given the droplet range. This value was an estimate, given that the diameters of the straws used in this study were on the order of magnitude of a few millimeters therefore the droplets formed should have a diameter of approximately the same order of magnitude. However, literature regarding fluid sprinklers has reported droplet diameters of between 0.1 mm to 1.0 mm (12). If the droplet size is estimated to be 0.1mm instead, the aerodynamic drag would be more significant, hence given the same droplet range, the exit velocity would be expected to be larger than the r=1.0 mm case. In Figure 11, the droplet radii of 0.05 mm and 0.5 mm are compared. Due to having a more significant drag force, the droplet range for r = 0.05mm is smaller for a given angular velocity, compared to that for r = 0.5mm, as shown in Figure 11 (a). Meanwhile, the droplet range is the quantity measured experimentally, and given the same measured droplet range, one would expect the exit velocity to be larger if the droplets are assumed to have a radius of 0.05 mm instead of 0.5 mm, as Figure 11 (b) shows. Both plots in Figure 11 show data of Ω and droplet range covering the values measured in the actual experiment, hence the data analyses would turn out significantly different if the droplet radius were considered to be 10 times smaller. However, since the current experimental analysis fits the theory well, the estimate that r=1 mm is more plausible.

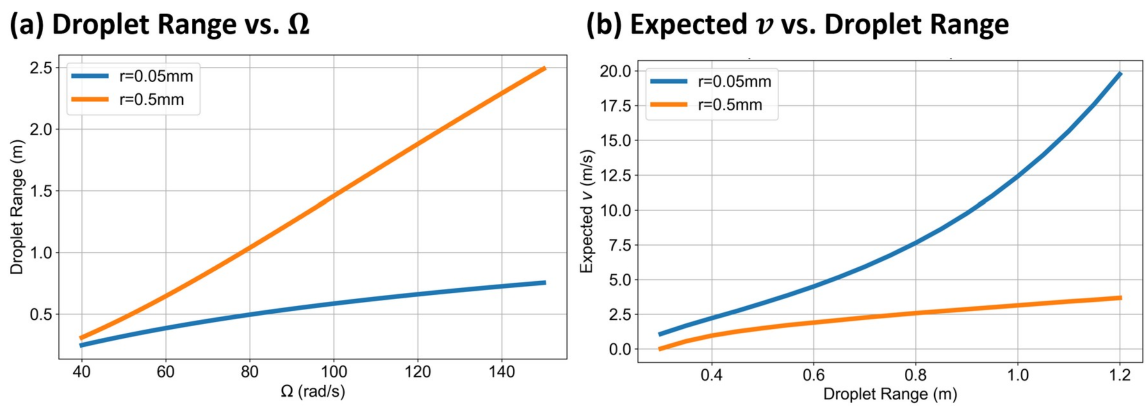

Figure 11. Comparison of droplet range, expected v(τ) and Ω. (a) The dependence of droplet range vs. angular velocity. Aerodynamic drag is more significant for smaller droplet radius, hence the r=0.05 mm curve is below the r=0.5 mm curve. (b) Relationship between expect v and droplet range, when the latter is measured experimentally. Given the same droplet range, one would expect the r=0.05 mm droplet to exit at a larger velocity due to the more significant air drag it experiences while airborne.

In the theoretical model, all parts of water, with a diameter of 2a, in the straw experience centrifugal force, hence the centrifugal force acts on the water with a diameter of 2a. Since a << l, the variation of centrifugal force along the radial direction is neglected. If, for some physical consideration, the centrifugal force should be considered to act on an effective diameter of "a" only, then the effect of the centrifugal force would be reduced by a factor of one fourth, as the volume of water that experiences the force is proportional to the square of the diameter. Therefore, the exit velocity, considering such geometrical anomaly, would be lower compared to the current model.

Theoretical considerations and practical applications

Practical lawn sprinklers are pressured at the inlet in order to provide larger coverage. The p_{init}, which is the pressure at the inlet, is typically around 30 psi to 50 psi, while it should not exceed 80 psi (13). Pressurizing water at the inlet is equivalent to setting the water at some initial velocity when entering the bottom of the straw, and such initial velocity can be calculated using Bernoulli's law. Let the

p_{init} be denoted as p_{init}, then the effective initial velocity v_{init} in the theoretical model is given by

$$v_{init} = (2p_{init}/\rho)^{1/2} \tag{16}$$

To create a larger coverage of water droplets, the pinit can be varied in a specified pressure range, since different inlet pressures correspond to different initial velocities when applied to the theoretical model. Retracing to equation (3), when there is a radial initial velocity of $dr(t=0)/dt = v_{init}\cos\theta$, the constant A' is nonzero. Differentiating equation (3) and setting it equal to $v_{init}\cos\theta$ at t=0 yields the value of A'

$$A' = v_{init} \cos\theta / \Omega' \tag{17}$$

Hence equation (4) should be modified to

$$r(t) = (v_{init}\cos\theta/\Omega') \sinh\Omega' t + (r_0 - r_{0c}) \cosh\Omega' t + r_{0c} \tag{18}$$

The time τ that the infinitessimal water segment exits the straw, found by setting $r(\tau)=l\cos(\theta)$, is solved numerically using Python's Scipy library. The radial component of the exit velocity can be found by evaluating the derivative of equation (18) at time τ, and $v(\tau)$ can be calculated accordingly. The remainder of the analysis is identical to that calculated without considering the p_{init}.

Here, a pulsatile p_{init} range of 20 psi to 80 psi is considered. Figure 12 presents data for p_{init} values of of 0 psi, 20 psi, 50 psi and 80 psi. In Figure 12 (a), it is observed that a larger p_{init} leads to a larger $v(\tau)$ by providing an initial flow velocity at the inlet. The variation of $v(\tau)$ with Ω declines with p_{init} since the total time of infinitesimal water segments accelerating inside the straw is smaller when the p_{init} is larger. Also, due to the initial velocity at the inlet caused by the p_{init}, water can exit the straw even if the straw itself is not rotating, hence the Ω-cutoff is not observed for nonzero p_{init} values. Figure 12 (b) shows that larger p_{init} also leads to a larger droplet range. The variation of droplet range with Ω is significant, even at large p_{inits}, due to the component of exit velocity caused by straw rotation, which is proportional to Ω. Figure 12 suggests that in practical lawn sprinkler scenarios, one can vary the p_{init} to create a larger coverage. For instance, by increasing the p_{init} from 20 psi to 80 psi, the range of water droplets can be increased from approximately 4 to 8 meters. If the straw pump is set spinning with a changeable angular velocity from 0 to 250 rad/s, the maximum droplet range can be extended to 9 meters, hence extending droplet range without raising the p_{init} to a high value, which may potentially damage the sprinkler. If the sprinkler must sprinkle water at a particular range, it is also possible to set the p_{init} at a rough value, and fine-tune the droplet range by varying Ω, since practically the variation of droplet range with Ω is easier to control.

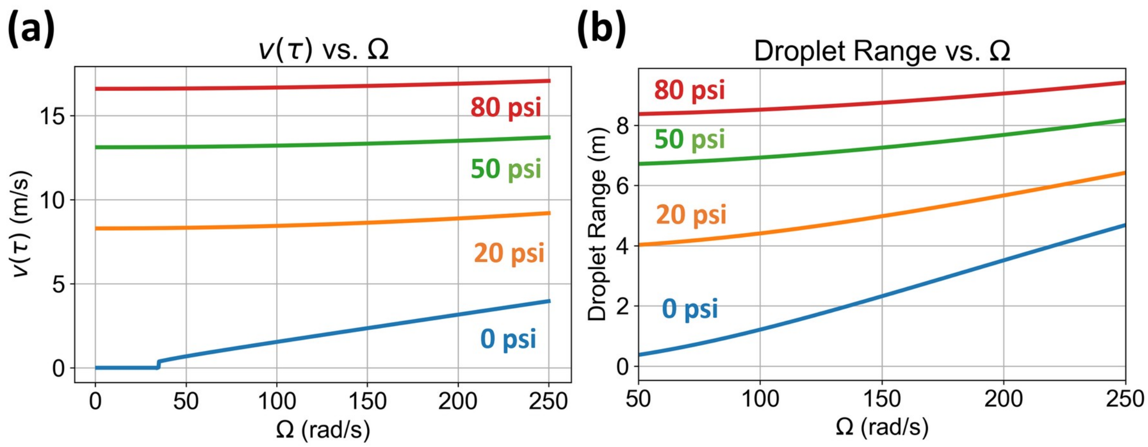

Figure 12. Effect of pinit on v(τ) and droplet range. The pinit values presented are of 0psi (no pinit), 20 psi, 50 psi and 80 psi. Parameters used for plotting are h_0=25 mm, l=70 mm, φ=60° and a=4 mm. (a) Plot of v(τ) vs. Ω shows that a larger pinit leads to a larger v(τ) by providing an initial flow velocity at the inlet. The variation of v(τ) with Ω declines with p_{init}. (b) Relationship of droplet range vs. Ω shows that larger p_{init} leads to a larger droplet range. The variation of droplet range with Ω is significant.

In fire sprinkler scenarios, sprinkler systems for fire control may use gravity fed or city pressurized water systems (14). The former method is accomplished by placing a water tank at a higher position, particularly useful in areas where reliable water pressure from the municipal supply is not available or when the building is located in a remote area. The latter method uses the water pressure provided by the municipal water supply to feed the sprinklers, which is common in urban areas with reliable and sufficient water pressure. In some cases, combined systems with both gravity-fed and city pressurized water systems are used in order to ensure that there is a backup when one of the systems fail.

Conclusion

Neglecting fluid effects, the dynamics of water in the triangular straw pump was modeled using point-mass mechanics by solving the equations of motion for an infinitesimal water segment. Then, Bernoulli's effect, viscosity and surface tension effects were qualitatively discussed and corrected for, since it was concluded that the former two are significant. These two factors were taken into consideration by calculating the pressure difference they contributed and calculating an effective gravitational acceleration for the point-mass model. The exit velocity could be determined experimentally by measuring the droplet range, taking air resistance into account. Based on the three sets of experiments conducted, it was found that experimental data for varying angular velocity, immersion depths and straw diameters agreed well with the theoretical corrected point-mass model, with minor deviations that could be attributable to low air pressure at the exiting vertex of the straw. It was also concluded that both the exit velocity and droplet range vary significantly with the tilt angle of the side of the straw, and it was shown theoretically that a maxima for both the quantities existed. The size of droplets was important when determining the exit velocity of water droplets experimentally. It was found that this size was approximately the same as that of the straw diameter. In practical applications, the range of water droplets could be increased by adding a p_{init}, which is equivalent to adding an initial velocity in the point-mass model. If the p_{init} was varied in a pulsatile manner, a larger coverage of water droplets could be achieved, and the spinning motion of the straw could both fine-tune and further increase the droplet range. The theoretical model is valuable for finding optimal designs for practical applications of water sprinklers.

Acknowledgements

I acknowledge my physics teacher Ms. Dai-Ching Jou for encouraging me to research this topic. She prepared the essential elements for the experiment apparatus. I also thank Professor Hung-Chih Kan of National Chung Cheng University for helpful comments on my theoretical model.

Abbreviations

Ω (rad/s): Angular velocity of the triangular straw, l (m): Side length of the triangular straw, a (m): Straw radius, h_0 (m): Straw immersion depth into water, v_{exit} (m/s): Exit velocity of water droplets, v_{th} (m/s): Theoretical prediction of the velocity component along the straw, u (n/s): The component of exit velocity caused by the rotation of the straw, φ (rad): Tilt angle.

References

1. Bureau of Energy Efficiency. (n.d.). *Chapter 6: Energy Efficiency in SMEs*. Bureau of Energy Efficiency, Ministry of Power, Government of India. https://www.beeindia.gov.in/sites/default/files/3Ch6.pdf

2. Monson, O. W. (1940). *The Homemade Centrifugal Pump*. Montana Extension Service Bulletin No. 185. https://zbook.org/read/ca6290_the-homemade-centrifugal-pump-montana-state-university.html

3. Ansell, D. (2009, April 19). *Pumping Straw - A Centrifugal Pump.* The Naked Scientists. https://www.thenakedscientists.com/get-naked/experiments/pumping-straw-centrifugal-pump

4. d'ArtofScience. (2014, March 2). *How to make a Water pump with a Straw* [Video]. YouTube. https://www.youtube.com/watch?v=yf1tSFXhnjw&t=99s&ab_channel=d%27ArtofScience

5. Villarino, M. B. (2008). *Ramanujan's Perimeter of an Ellipse*. Escuela de Matematica, Universidad de Costa Rica. https://doi.org/10.48550/arXiv.math/0506384

6. Virtanen, P., Gommers, R., Oliphant, T. E., Haberland, M., Reddy, T., Cournapeau, D., et al. (2020) SciPy 1.0: *Fundamental Algorithms for Scientific Computing in Python. Nature Methods*,

17(3), 261-272. https://doi.org/10.1038/s41592-019-0686-2

7. Gutierrez, J., Royals, A., Hasan, J., Venditti, R., Pal, L. (2019). *Evaluation of Paper Straws versus Plastic Straws: Development of a Methodology for Testing and Understanding Challenges for Paper Straws*. Bioresources. 14 (4). 8345-8363. http://dx.doi.org/10.15376/biores.14.4.8345-8363

8. User "Harold Jans". (2023). *Darcy Friction factor for Re between 10 and 10e8 for values of relative roughness* [Digital image]. Wikimedia Commons. https://commons.wikimedia.org/wiki/File:Darcy_Friction_factor_for_Re_between_10_and_10E8_for_values_of_relative_roughness.svg

9. Nakayama, Y. (2018). *Introduction to Fluid Mechanics*. Elsevier Science. ISBN: 9780081024386. LCCN: 2018302740.

10. National Aeronautics and Space Administration. (n.d.). Air Mass & Density. NASA Earthdata. https://www.earthdata.nasa.gov/topics/atmosphere/atmospheric-pressure/air-mass-density#:~:text=Pure%2C%20dry%20air%20has%20a,a%20pressure%20of%20101.325%20kPa

11. Wrachien, D., Lorenzini, G., Mambretti, S., Medici, M. (2016). *Fluid Dynamics of Sprinkler Spay Flow : Classical and Quantum Trajectories*. Proceedings of the 44th International Symposium On Agricultural Engineering: Actual Tasks on Agricultural Engineering, Opatija, Croatia. 85-98, ref. 33. https://www.researchgate.net/publication/295911830_Fluid_Dynamics_of_Sprinkler_Spay_Flow_Classical_and_Quantum_Trajectories

12. Conevski, S., Aleixo, R., Guerrero, M., Ruther, N. (2020). Bedload velocity and backscattering strength from mobile sediment bed: A laboratory investigation comparing bistatic versus monostatic acoustic configuration. *Water,* 12(12), 3320. https://doi.org/10.3390/w12123320

13. Nature's Helper. (n.d.). What is the typical water pressure for a sprinkler system? Nature's Helper. https://www.natureshelperinc.com/blog/what-is-the-typical-water-pressure-for-a-sprinkler-system/

14. National Fire Protection Association. (2021, June 7). Types of water supplies for fire protection systems. NFPA. Retrieved June 30, 2024, from https://www.nfpa.org/news-blogs-and-articles/blogs/2021/06/07/types-of-water-supplies